nature communications

Article

https://doi.org/10.1038/s41467-025-66093-0

Divergent synthesis of *Haplomitrium* diterpenoids via a late-stage biomimetic skeletal reorganization approach

Received: 6 August 2025

Accepted: 30 October 2025

Published online: 15 December 2025

Check for updates

Zong-Xu Gao[1], Chenyingchun Su[1], Hai-Xia Zhang[1], Yue-Qing Zhang[1], Xiao-Xue Chen[1], Xu-Yuan Liu[1], Ai-Xia Cheng[1], Ze-Jun Xu[1,2] ✉ & Hong-Xiang Lou[1,2,3] ✉

Labdane-type terpenoids, the large super-family of diterpenoids, exhibit diverse biological significance. Labdane-derived hapmnioide-type diterpenoids, which have been identified as chemical markers for *Haplomitrium* liverwort, show potent anti-inflammatory and allelopathic activities. Biosynthetically, their structural complexity and diverse carbon skeletons arise from cascade ring mutations. We describe total synthesis of seven typical *Haplomitrium* diterpenoids through late-stage biomimetic skeletal reorganization, featuring 1,2-acyl migration, tandem C5-isomerization/aldol/*retro*-Claisen reactions, and light-initiated [2 + 2] cyclization. A diastereoselective intramolecular Diels–Alder reaction is employed to rapidly assemble the common labdane core skeleton. The 1,2-migration of the labdane intermediate is developed to synthesize hapmnioide A and haploide O. Furthermore, the tandem C5-isomerization/aldol/*retro*-Claisen reactions and light-initiated [2 + 2] cyclization of the common labdane intermediate enables the reconstruction of haploide C and haplomitrins A/C, respectively. The synthetic work provides mechanistic insights into the biosynthesis of hapmnioide-type diterpenoids. Further investigations of the 1,2-acyl migration of other terpenoids demonstrate the general and potential applicability of such late-stage rearrangements for the synthesis of homologous molecules.

Terpenoid natural products have long been valuable sources of inspiration for developing therapeutically useful molecules[1,2]. Labdanes represent a structurally unique diterpenoid subclass encompassing pharmaceutically significant metabolites[3], including andrographolide, forskolin, and nimbolide. Its structural diversity stems from its assembly line-like biosynthesis, where the building block is first assembled, followed by structural diversification. Representative modes of scaffold diversification include skeletal rearrangement, redox processes, appendages adding, dimerization, or combinations thereof. Among these, skeletal rearrangement stands out as it can generate entirely distinct skeletal frameworks, often leading to new families of terpenoids. This biosynthetic logic has provided significant inspiration for chemists in the development of synthetic strategies[4–17].

1,2-Migration is extensively involved in the biosynthetic skeletal rearrangement of terpenoids, the classic example of which is 1,2-H and 1,2-methyl migration. Carbocation-mediated 1,2-migration rearrangements, particularly Wagner-Meerwein, pinacol, and

[1]Department of Natural Products Chemistry, Key Laboratory of Chemical Biology (Ministry of Education), School of Pharmacy, Shandong University, Jinan, Shandong, China. [2]State Key Laboratory of Discovery and Utilization of Functional Components in Traditional Chinese Medicine, Shandong University, Jinan, China. [3]Joint research institute of Medical and Pharmaceutical Sciences, Qilu Hospital of Shandong University, Shandong University, Jinan, China. ✉e-mail: xuzejun@sdu.edu.cn; louhongxiang@sdu.edu.cn

https://doi.org/10.1038/s41467-025-66093-0

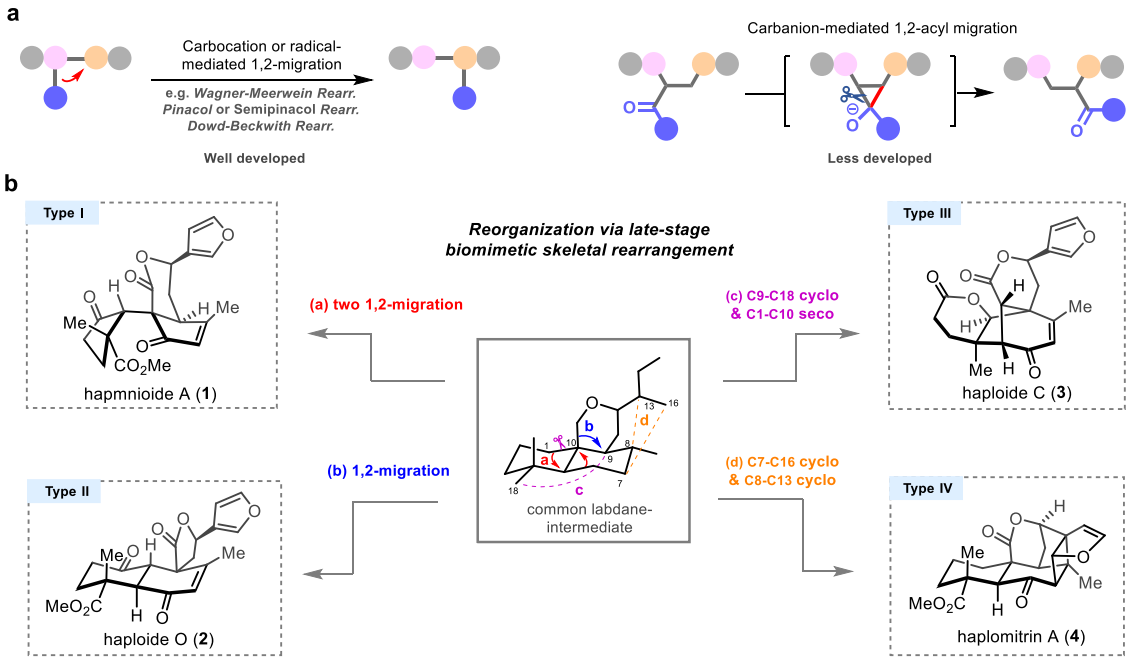

Fig. 1 | Background and our synthesis plan of the structurally diverse *Haplomitrium* diterpenoids. a Typical 1,2-alkyl/aryl shift involved in natural product biomimetic synthesis. **b** Our bioinspired skeletal reorganization strategy for the synthesis of structurally diverse *Haplomitrium* diterpenoids. rearr. rearrangement.

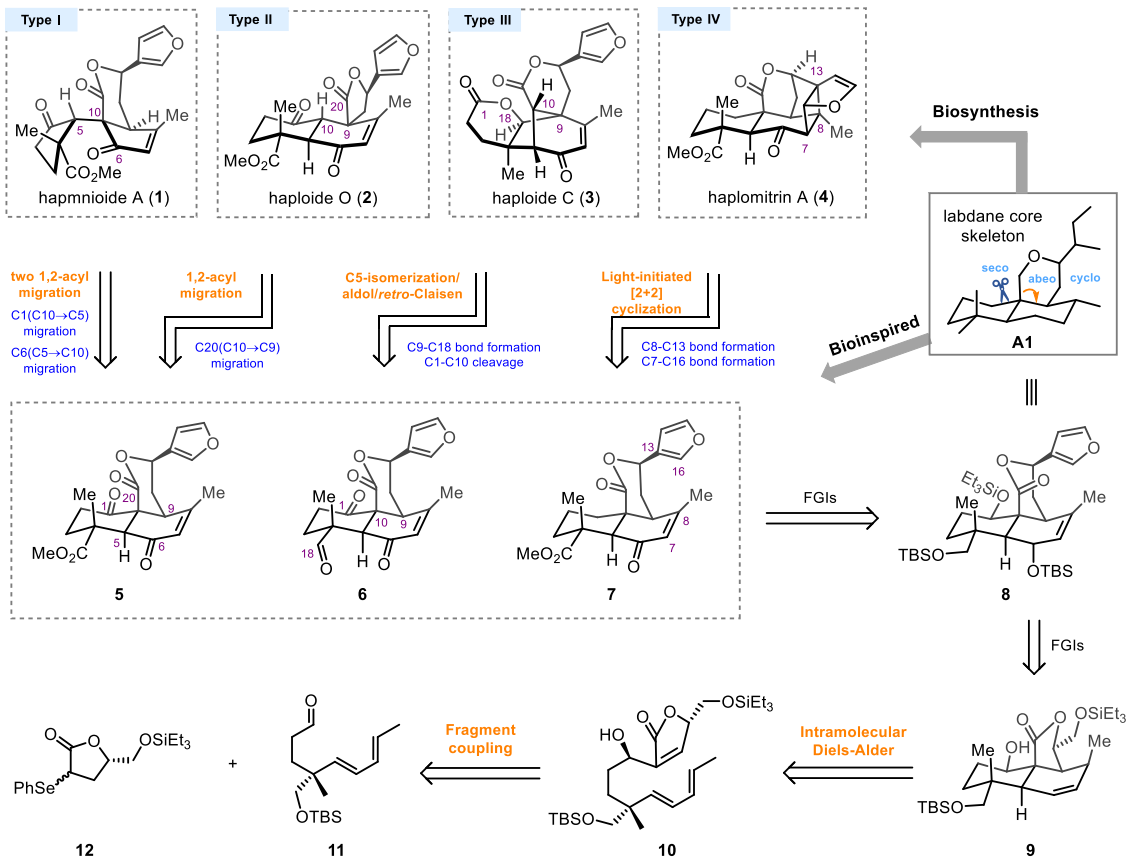

Fig. 2 | Retrosynthetic analysis. The retrosynthetic analysis of *Haplomitrium* diterpenoids is based on a late-stage bioinspired skeletal reconstruction approach. FGI functional group interconversion, TBS *tert*-butyldimethylsilyl.

semipinacol rearrangements, have been effectively utilized, demonstrating their powerful potential in the synthesis of terpenoids[18–25]. In contrast, examples of late-stage 1,2-migration rearrangements of the polycyclic ring systems proceeding via unconventional reaction mechanisms, in which carbocations might not be involved, remain scarce[26–29]. The discovery and utilization of migration patterns, particularly carbanion-mediated 1,2-acyl migration (Fig. 1a)[30–35], remain urgent pursuits, and elucidating these

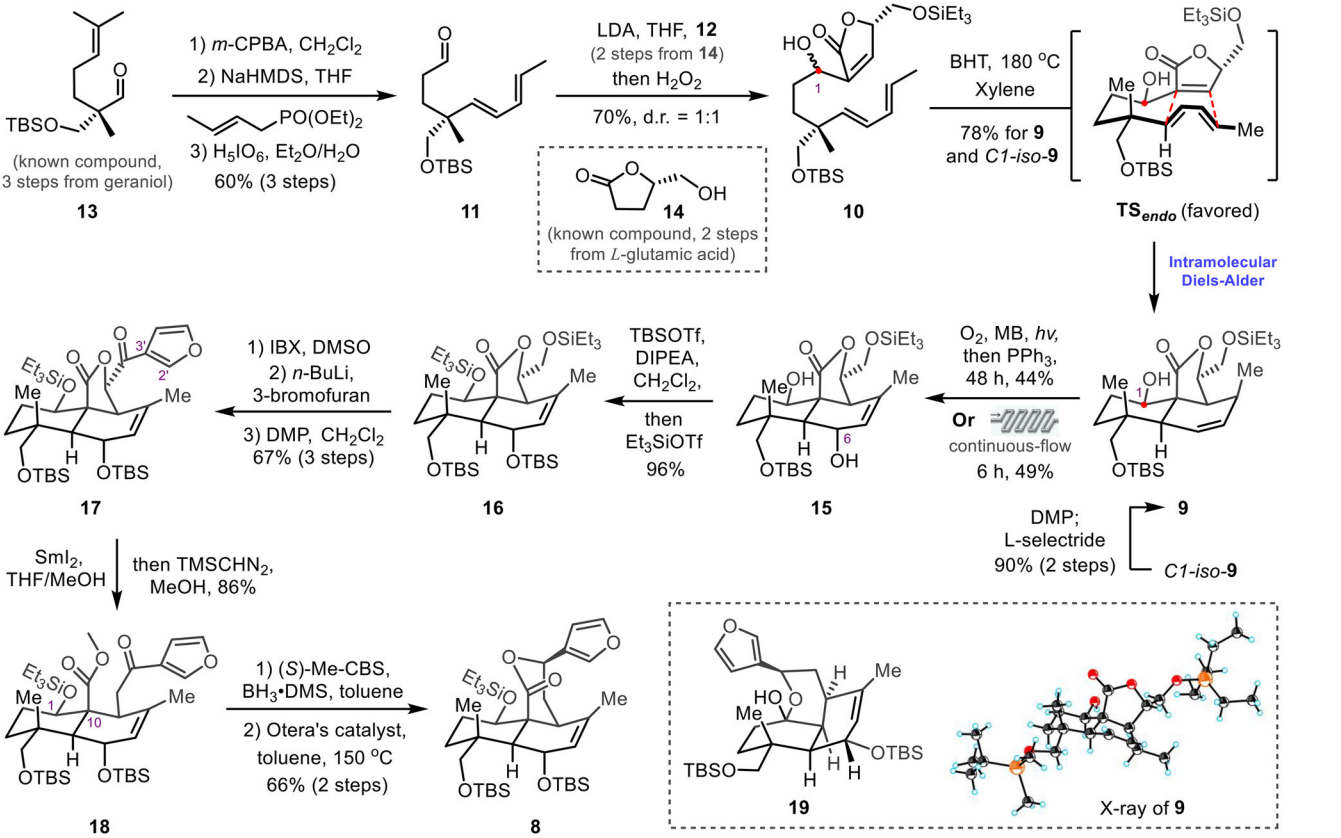

Fig. 3 | Synthesis of the common intermediate 8. *m*-CPBA 3-chloroperoxybenzoic acid, NaHMDS sodium bis(trimethylsilyl)amide, THF tetrahydrofuran, LDA lithium diisopropylamide, BHT 2,6-di-*tert*-butyl-4-methylphenol, MB methylene blue, TBSOTf *tert*-butyldimethylsilyl trifluoromethanesulfonate, DIPEA N, N-diisopropylethylamine, IBX 2-iodoxybenzoic acid, DMSO dimethyl sulfoxide, DMP Dess–Martin periodinane, $TMSCHN_2$ (trimethylsilyl)diazomethane, Me-CBS 5,5-diphenyl-2-methyl-3,4-propano-1,3,2-oxazaborolidine.

skeletal rearrangements is of perennial importance in natural products chemistry.

Since 2016, we have islolated a series of extensively rearranged and highly oxidized labdane-type diterpenoids (**1**–**4**, **7**, **34**, and **36**) from the Chinese liverwort *Haplomitrium mnioides*, which show potent anti-inflammatory and allelopathic activities[36–39]. Structurally, hapmnioide A (**1**), haploide C (**3**), and haplomitrin A (**4**) feature unique 1,1′-bicyclopentyl, bicyclo[3,2,1]octane, and tetracyclo[7.4.1.0^{2,7}.0^{11,14}]tetradecane ring systems, respectively. Despite great progress in labdane synthesis, however, the development of unified strategies toward the collective construction of biogenetically related labdane-type diterpenoid skeletons is still limited[40–45]. In this work, inspired by the skeletal rearrangement in their biosynthetic pathways and in connection with our interest in divergent synthesis[46–48], we envisage that these related *Haplomitrium* diterpenoids can be forged through late-stage biomimetic skeletal reorganization of the common labdane scaffold, featuring previously unreported tandem 1,2-acyl migration (Fig. 1b). Further investigations of 1,2-acyl migrations on other terpenoid scaffolds demonstrate the applicability of this late-stage remodeling strategy for accessing complex molecules.

Results

Retrosynthetic analysis

Our synthesis plan, which is inspired by the biosynthetic pathways of *Haplomitrium* diterpenoids, is shown in Fig. 2. We envisioned that the 1,1′-bicyclopentyl carbon framework of hapmnioide A (**1**) could be derived successively from trans-decalin **5**, employing two consecutive stereospecific 1,2-acyl migrations of the labdane-type core skeleton at C-1 and C-6[49,50]. Similarly, haploide O (**2**) could also be accessed via one stereospecific 1,2-acyl migration at C-20 from **5**. To construct the bicyclo[3,2,1]octane of haploide C (**3**), we proposed that the tandem C5-isomerization/aldol/*retro*-Claisen reactions of aldehyde **6** are responsible for the direct assembly of **3**. Highly rigid haplomitrin A (**4**) can be straightforwardly synthesized via an intramolecular light-initiated [2+2] cycloaddition of enone **7**[37,51]. Compounds **5**–**7** all feature the same labdane core skeleton. Thus, the proposed biosynthetic precursor **8** could serve as a common advanced precursor for quickly synthesizing **5**–**7** via functional group interconversions. Additionally, δ-lactone **8** could be derived from γ-lactone **9** by the installation of the furan-containing side chain, and the trans-decalin framework of **9** could be accessed by an *endo*-selective intramolecular Diels–Alder (IMDA) reaction of trienolide **10**, concomitantly establishing the pivotal C10 quaternary carbon stereogenic center[52]. Trienolide **10** can be rapidly generated by the coupling of aldehyde **11** with selenolactone **12**, which should be readily prepared from known compounds **13** and **14**, respectively[53–55].

Synthesis of the common intermediate 8

Our synthesis commenced with the preparation of the chiral aldehyde **11** (Fig. 3), which was obtained via a three-step sequence of the known aldehyde **13** (prepared from geraniol in three steps[53,54]; see Supplementary Fig. 1a) in 60% overall yield involving epoxidation, Horner–Wadsworth–Emmons reaction, and oxidative cleavage. Subsequently, aldehyde **11** condensed with the lithium enolate of selenolactone **12** (prepared from *L*-glutamic acid in four steps[55]; see Supplementary Fig. 1b), followed by oxidation to afford trienolide **10** with 70% yield and 1:1 selectivity at C1. Trienolide **10** underwent a highly stereospecific IMDA reaction to form trans-decalin **9**, the

https://doi.org/10.1038/s41467-025-66093-0

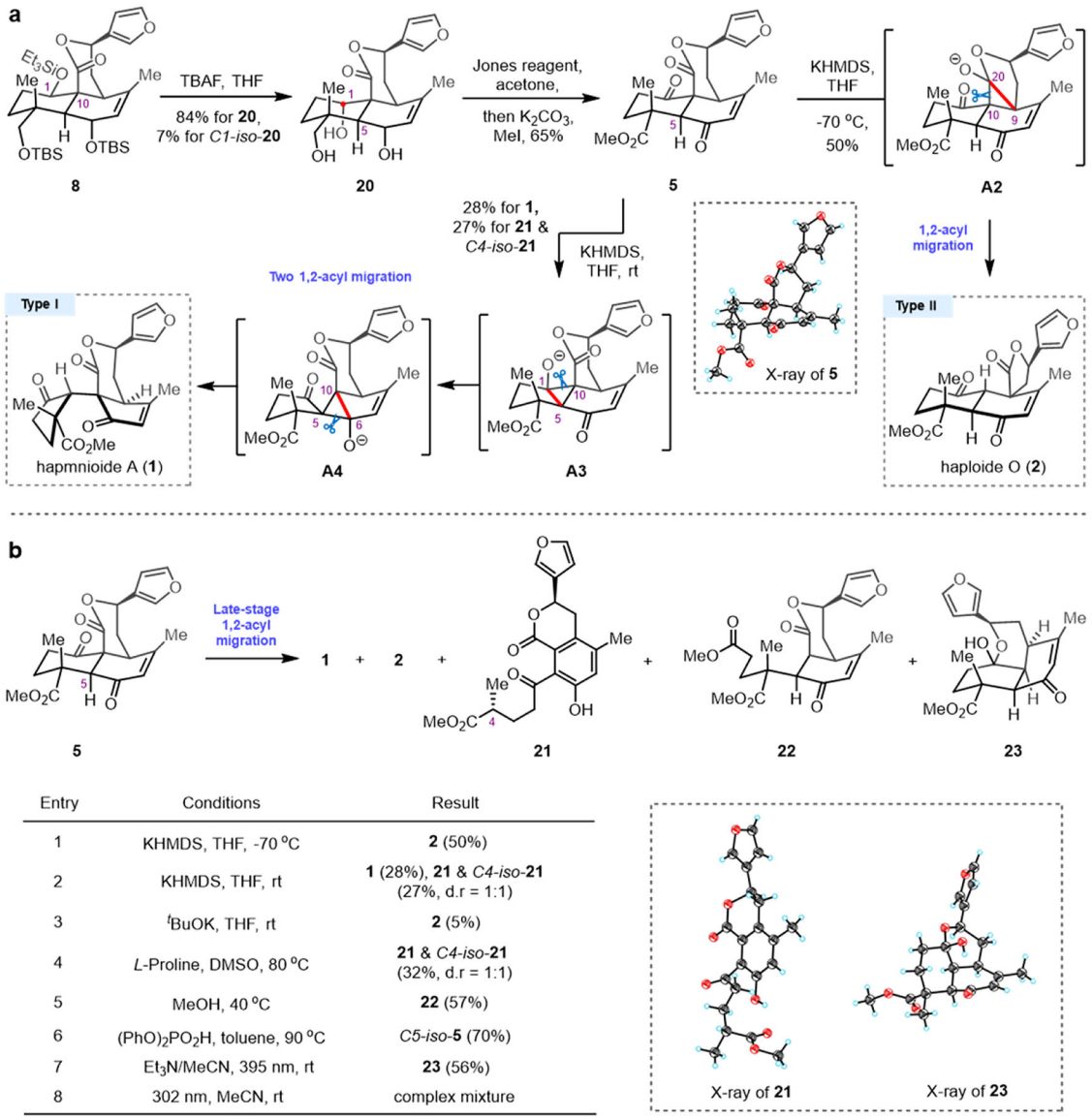

Entry	Conditions	Result
1	KHMDS, THF, -70 °C	**2** (50%)
2	KHMDS, THF, rt	**1** (28%), **21** & *C4-iso*-**21** (27%, d.r = 1:1)
3	^{t}BuOK, THF, rt	**2** (5%)
4	*L*-Proline, DMSO, 80 °C	**21** & *C4-iso*-**21** (32%, d.r = 1:1)
5	MeOH, 40 °C	**22** (57%)
6	$(PhO)_2PO_2H$, toluene, 90 °C	*C5-iso*-**5** (70%)
7	Et_3N/MeCN, 395 nm, rt	**23** (56%)
8	302 nm, MeCN, rt	complex mixture

Fig. 4 | Synthesis of hapmnioide A (1) and haploide O (2). a Divergent total synthesis of hapmnioide A (**1**) and haploide O (**2**) from the common intermediate **8**. **b** Optimization of reaction conditions for pivotal 1,2-acyl migration. TBAF tetrabutylammonium fluoride, KHMDS potassium bis(trimethylsilyl)amide, rt room temperature.

structure of which was confirmed by X-ray crystallography[52,56–60]. The selectivity was attributed to steric effects, which were mediated by the *endo*-selective transition state (**TS**$_{endo}$). The isomeric product *C1-iso*-**9**, derived from the cyclization of *C1-iso*-**10**, could be converted to **9** via a two-step sequence involving oxidation and selective reduction using L-selectride in 90% yield. To introduce the C6 oxidation state, a singlet oxygen-mediated ene reaction of **9** was employed, yielding allyl alcohol **15** with moderate regioselectivity[61]. Notably, this transformation demonstrated a reduced reaction time and enhanced productivity when conducted in continuous-flow mode (see Supplementary Fig. 1c).

We then introduced the furan-containing side chain to **15**. Subsequent one-pot selective silyl protection of the C6- and C1-hydroxy groups of **15** furnished silyl ether **16**. Triethylsilyl ether **16** was then subjected to IBX-mediated selective desilylation/oxidation to generate an unstable aldehyde intermediate[62], which was treated with the C3′-lithiated furan, and further oxidation with DMP yielded furyl ketone **17**. The base plays a key role in determining the regioselectivity of furan lithiation, where *n*-butyllithium predominantly facilitates lithiation at the C3′ position of the furan ring (see Supplementary Fig. 1d). The C–O bond adjacent to the ketone in **17** was reduced with SmI_2, and subsequent methylation of the resulting carboxylic acid using $TMSCHN_2$ provided methyl ester **18**. Notably, quenching SmI_2-mediated reduction with dilute HCl efficiently removed the C1-hydroxy triethylsilyl group in **17**, resulting in fused cyclic ketal formation (see Supplementary Fig. 1e). Finally, ketone **18** was transformed into key precursor **8** via Corey-Bakshi-Shibata reduction followed by Otera lactonization[63]. Interestingly, during lactone ring closure attempts, degradation product **19** was observed under basic conditions (K_2CO_3/EtOH), arising from C1-C10 bond cleavage (see Supplementary Fig. 1f).

Synthesis of hapmnioide A (1) and haploide O (2)

Next, we proceeded to synthesize hapmnioide A (**1**) and haploide O (**2**) using the common labdane-type intermediate **8** (Fig. 4). We first modulated the oxidation state of **8** to access the key substrate **5**, which is required for the 1,2-acyl migration reaction. Tetrabutylammonium fluoride (TBAF) was employed to remove all three silyl protecting groups in **8**, exposing the hydroxyl groups at the C1, C6, and C18 positions in one step. Surprisingly, the major product obtained was the

https://doi.org/10.1038/s41467-025-66093-0

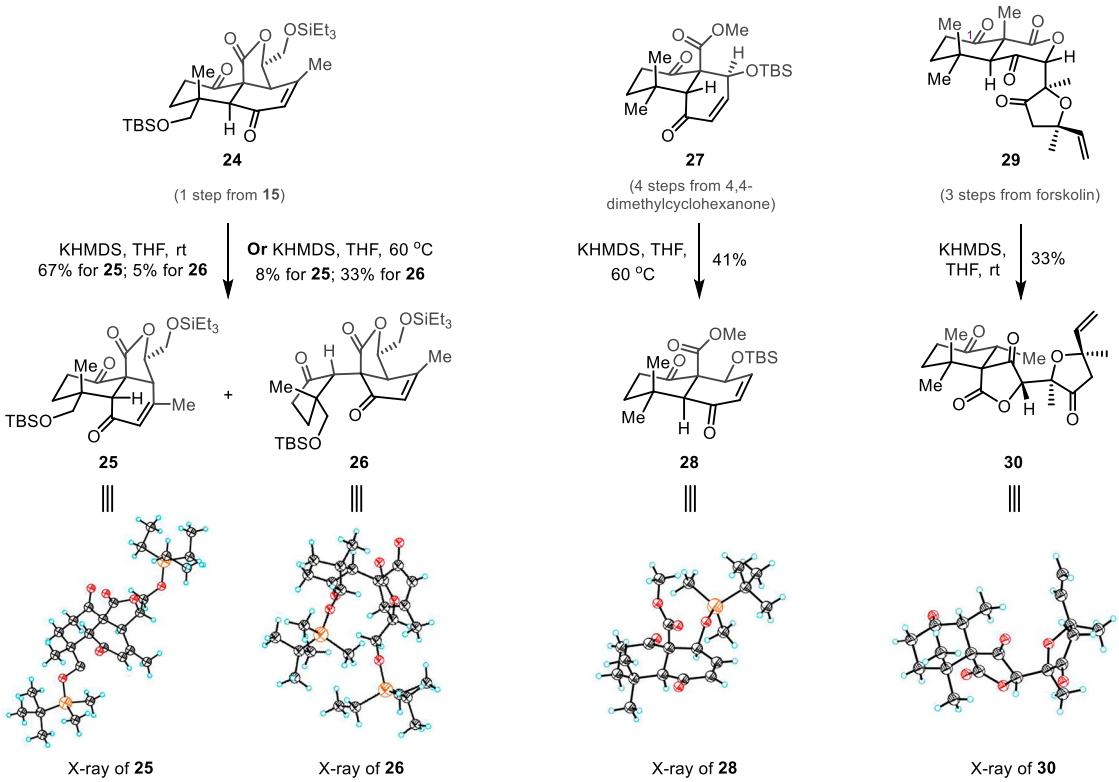

Fig. 5 | Late-stage 1,2-acyl migration rearrangements of polycyclic terpenoids. KHMDS potassium bis(trimethylsilyl)amide, rt room temperature, THF tetrahydrofuran.

C1 hydroxyl isomer **20**, which was likely formed via a *retro*-aldol/aldol process (see Supplementary Fig. 2b)[64], analogous to the C1–C10 bond cleavage observed in the formation of degradation product **19**. This further highlights the sterically congested environment at C10, which predisposes the C1–C10 bond to cleavage. Treatment of triol **20** with Jones reagent, followed by one-pot methylation of the resulting carboxylic acid, afforded methyl ester **5** in 65% yield, with its structure unequivocally confirmed by X-ray crystallographic analysis.

With the proposed biogenetic precursor **5** synthesized, we then systematically investigated its conversion to hapmnioide A (**1**) and haploide O (**2**), with the optimal conditions summarized in Fig. 4b[49,50]. To our delight, treatment of **5** with KHMDS at −70 °C induced stereospecific 1,2-acyl migration at C-20 through intermediate **A2**, affording haploide O (**2**) in 50% yield (Fig. 4b, entry 1). Interestingly, increasing the temperature to ambient conditions facilitated sequential stereospecific 1,2-acyl migrations through intermediates **A3** and **A4**, yielding hapmnioide A (**1**) together with aromatized side products **21** and *C4-iso*-**21** (Fig. 4b, entry 2, the structure of **21** was confirmed by X-ray crystallography). The formation of **21** and *C4-iso*-**21** proceeds through a C-1 1,2-acyl migration followed by *retro*-Michael cleavage of the C4-C5 bond (see Supplementary Fig. 2c). Higher reaction temperatures are needed, presumably due to the high TS energy barrier of **A3**[65]. Owing to competing reaction pathways, efforts to increase the yield of hapmnioide A (**1**) failed (Fig. 4b, entries 3 and 4). The spectroscopic data for synthesized hapmnioide A (**1**) and haploide O (**2**) matched those reported in the literature[36,38]. Notably, β-ketoester **5** was unstable, and underwent *retro*-Claisen cleavage to yield product **22** during reduced-pressure distillation (Fig. 4b, entry 5). Treatment of **5** with $(PhO)_2PO_2H$ provided the C5-isomerized product *C5-iso*-**5** in 70% yield (Fig. 4b, entry 6)[42]. Photochemical strategies have been extensively employed in acyl migration processes[35,66,67], prompting our investigation of diverse irradiation conditions. Interestingly, visible light irradiation (395 nm) of compound **5** with triethylamine triggered decarboxylative degradation, affording product **23** (structure unequivocally confirmed by X-ray analysis). Notably, light irradiation is indispensable for this transformation. The higher-energy UV light (302 nm) caused substantial decomposition of **5** (Fig. 4b, entries 7 and 8).

Late-stage 1,2-acyl migrations of polycyclic terpenoids

We further validated the late-stage 1,2-acyl migration rearrangements of labdane-type terpenoids or analogs to skeletal reorganization. As exemplified in Fig. 5, treatment of γ-lactone **24** (prepared from **15** in one step; see Supplementary Fig. 3a), whose five-membered lactone moiety resisted 1,2-ester migration, with KHMDS at room temperature afforded isomerized product **25** as the major species. Consistent with δ-lactone **5**, the reaction pathway demonstrated significant temperature sensitivity, impacting the reaction selectivity. When the temperature was increased to 60 °C, two consecutive stereospecific 1,2-acyl migrations predominated, resulting in 1,1′-bicyclopentyl **26** as the major product. To further investigate the impact of γ-lactones on these rearrangement processes, cis-decalin **27** was prepared from 4,4-dimethyl cyclohexanone in four steps to obtain the 1,2-ester migration product (see Supplementary Fig. 3b)[68]. Interestingly, exposure of the open-chain methyl ester **27** to KHMDS conditions yielded only the isomerized product **28**, even at elevated temperatures. We further incorporated the ester moiety into the bicyclic framework, obtaining trans-[6.6]-bicyclic δ-lactones **29** from forskolin in three steps (see Supplementary Fig. 3c)[69]. While treatment of **29** with KHMDS at room temperature provided the 1,2-ester migration product **30** in 33% yield. All the rearranged molecules (**25**, **26**, **28**, and **30**) were unambiguously characterized by comprehensive NMR studies, and their structures were further confirmed by X-ray crystallographic analysis.

https://doi.org/10.1038/s41467-025-66093-0

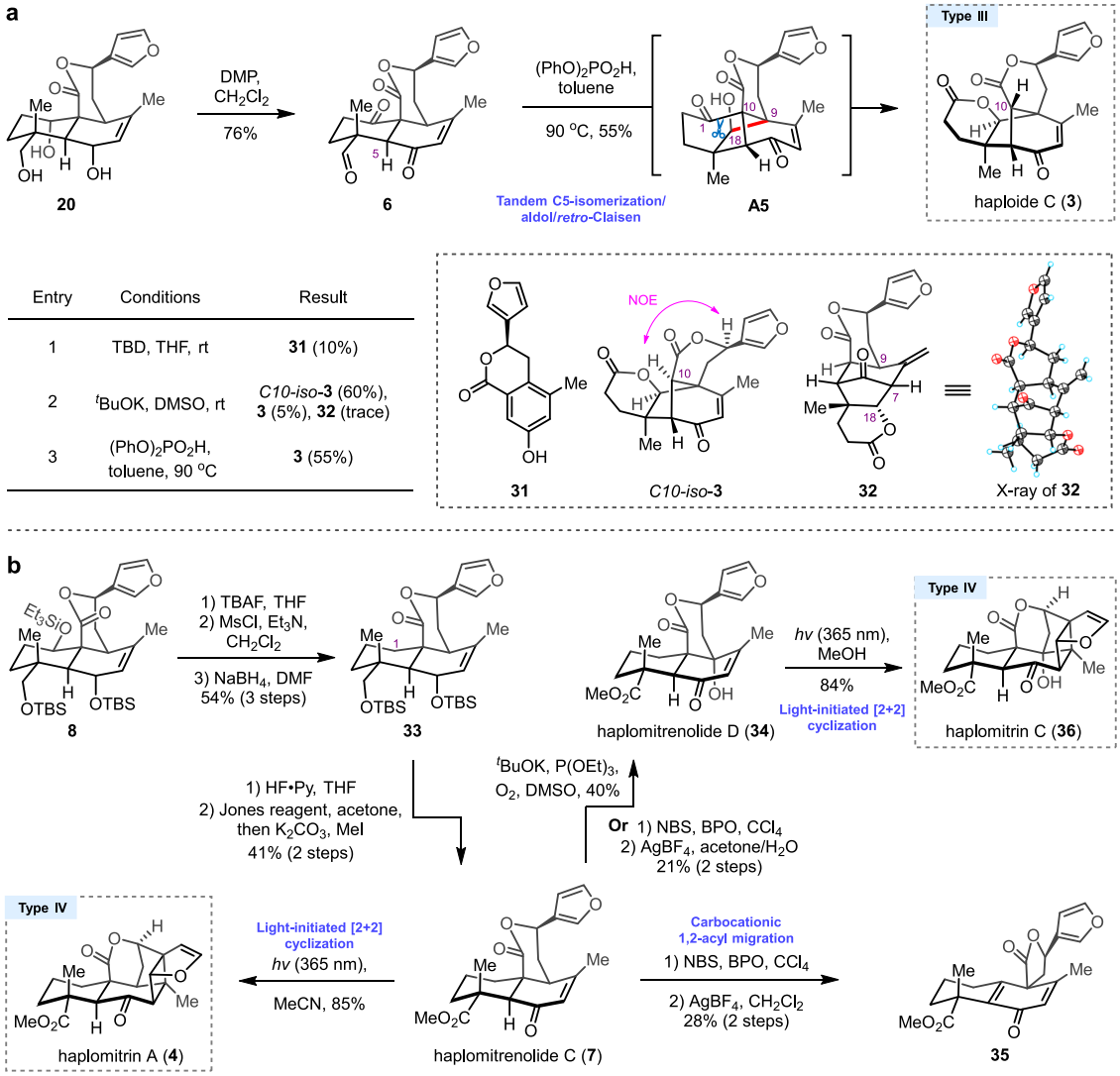

Fig. 6 | Synthesis of haploide C (3), haplomitrenolides C/D (7/34), and haplomitrins A/C (4/36). a Total synthesis of haploide C (**3**) enabled by the tandem C5-isomerization/aldol/*retro*-Claisen reaction of **6**. **b** Divergent total syntheses haplomitrenolides C/D (**7**/**34**) and haplomitrins A/C (**4**/**36**) from the common intermediate **8**. DMP Dess–Martin periodinane, TBD 1,5,7-triazabicyclo[4.4.0]dec-5-ene, DMSO dimethyl sulfoxide, TBAF tetrabutylammonium fluoride, MsCl methanesulfonyl chloride, DMF N,N-dimethylformamide, Py pyridine, NBS N-bromosuccinimide, BPO dibenzoyl peroxide.

Synthesis of haploide C (3)

We next pursued the biomimetic synthesis of haploide C (**3**), featuring a bicyclo[3.2.1]octane scaffold (Fig. 6a). The key aldehyde **6** was synthesized from triol **20** via DMP-mediated oxidation, enabling exploration of the tandem C5-isomerization/aldol/*retro*-Claisen cascade. Notably, under TBD catalysis, B-ring aromatized product **31** was obtained, presumably via a *retro*-Claisen/*retro*-Michael/aromatization cascade reaction (Fig. 6a, entry 1; see Supplementary Fig. 3d). Employing potassium *tert*-butoxide afforded *C10-iso*-**3** (60% yield) and haploide C (**3**) (5% yield), along with the C7-C18 cyclized product **32**, the structure of which was established by X-ray crystallography (Fig. 6a, entry 2). The proposed formation pathways for compounds *C10-iso*-**3** and **32** are detailed in Supplementary Fig. 3e. Attempts to isomerize the C10 position of *C10-iso*-**3** were unsuccessful. Systematic evaluation of base-mediated condensation protocols revealed limited efficiency, prompting us to explore an acid-catalyzed strategy. Fortunately, treatment of aldehyde **6** with the Brønsted acid $(PhO)_2PO_2H$ successfully afforded haploide C (**3**) in 55% yield[42]. The observed facial selectivity at C18 could be attributed to the double hydrogen bonding coordination of the phosphinic acid catalysts (see Supplementary Fig. 3f)[70]. The spectroscopic data of the synthesized haploide C (**3**) were consistent with the literature reports[38].

Synthesis of haplomitrins A/C (4/36)

Given the highly rigid tetracyclic framework of haplomitrins, we first prepared haplomitrenolide C (**7**), bearing a C1-methylene group, for [2 + 2] cycloaddition attempts[37,51,71] (Fig. 6b). Selective C1 triethylsilyl ether deprotection using 1 equiv. TBAF, followed by mesylation and $NaBH_4$ reduction to convert the hydroxyl group to a methylene group, formed **33** in 54% yield over three steps. Sequential deprotection of the C6 and C18 silyl groups using HF•Py, followed by Jones oxidation and methyl esterification, afforded haplomitrenolide C (**7**). To our delight, irradiation of haplomitrenolide C (**7**) with 365 nm light in MeCN efficiently formed haplomitrin A (**4**) in 85% yield (ring opening of the δ-lactone moiety occurred in ethanol). The synthesis of haplomitrin C (**36**) requires hydroxylation at C9. Exposure of **7** to $^tBuOK/P(OEt)_3$ under O_2 directly provided haplomitrenolide D (**34**) in 40% yield[72]. Alternatively, this enone allylic hydroxylation could be accomplished via a two-step bromination/hydrolysis sequence in 21% yield. Notably, the choice of silver salt and solvent is crucial, and the C9-brominated

intermediate was efficiently converted to compound **35**, constituting the haploide O (**2**) skeleton via carbocation-mediated 1,2-acyl migration in $AgBF_4$/dichloromethane (see Supplementary Fig. 4a)[73,74]. Similarly, irradiation of haplomitrenolide D (**34**) with 365 nm light afforded haplomitrin C (**36**) in 84% yield. The NMR spectroscopic data of these synthetic natural products matched those reported in the literature[38].

Discussion

In summary, we have developed a bioinspired and divergent synthesis strategy that enables total synthesis of seven biogenetically related *haplomitrium* diterpenoids: hapmnioide A, haploides C/O, haplomitrenolides C/D, and haplomitrins A/C. The key features of this route include a diastereoselective IMDA reaction to rapidly assemble the labdane core skeleton. 1,2-Acyl migration of the labdane core skeleton was employed to synthesize hapmnioide A and haploide O. Two consecutive stereospecific 1,2-acyl migrations have been observed. Furthermore, the tandem C5-isomerization/aldol/*retro*-Claisen reactions and light-initiated [2+2] cyclization of the common labdane skeleton enable the construction of haploide C and haplomitrins A/C, respectively. Further investigations of 1,2-acyl migration on other labdane-type terpenoids or analogs demonstrated the applicability of such late-stage rearrangements for the synthesis of structurally diverse small molecules. The synthetic work provides insights into in labdane-type terpenoid assembly, revealing that aldol-like reaction play a significant role in the biosynthesis of *haplomitrium* diterpenoids. The strategies described to prepare complex molecular architectures will be applicable to the assembly of other structurally related terpenoids.

Methods

Synthesis of hapmnioide A (1)

Under argon atmosphere, to a solution of compound **5** (7.8 mg, 20.2 µmol, 1.0 equiv.) in anhydrous THF (2.0 mL) was added KHMDS (10.1 µL, 1 M in anhydrous THF, 10.1 µmol, 0.5 equiv.) at 0 °C, followed by 5 min stirring at the same temperature. The reaction mixture was warmed to room temperature and stirred for 24 h before quenched with saturated aqueous ammonium chloride (2 mL). The aqueous layer was extracted with ethyl acetate (5 mL ×3). The combined organic layers were washed with brine (10 mL), dried over anhydrous sodium sulfate, filtered, concentrated and purified by flash column chromatography (dichloromethane/methanol = 50/1) to yield **1** (2.2 mg, 28%) and **21** & *C4-iso*-**21** (2.1 mg, 27%) as white solids.

Synthesis of haploide C (3)

To a solution of compound **6** (6.0 mg, 16.8 µmol, 1.0 equiv.) in anhydrous toluene (1.7 mL) was added $(PhO)_2PO_2H$ (5.1 mg, 20.2 µmol, 1.2 equiv.) under argon atmosphere. The reaction was stirred at 90 °C overnight. The mixture was concentrated in vacuo and purified by flash column chromatography (petroleum ether/ethyl acetate = 1/2) to yield **3** (3.3 mg, 55%) as a white solid.

Data availability

Details of the experimental procedures, spectral data, and full characterizations are provided in the Supplementary Information. The X-ray crystallographic coordinates for structures reported in this study have been deposited at the Cambridge Crystallographic Data Centre (CCDC) under deposition numbers CCDC 2447365 (**5**), 2447362 (**9**), 2447368 (**21**), 2447370 (**23**), 2447364 (**25**), 2447369 (**26**), 2447371 (**28**), 2447372 (**30**), 2447363 (**32**), 2447367 (**S8**), and 2447366 (**S9**). These data can be obtained free of charge from The Cambridge Crystallographic Data Centre via www.ccdc.cam.ac.uk/data_request/cif. A cyclic trinuclear Ag(I) complex (Ag_3Pz_3) as a crystalline mate for compounds **21**, **23**, **26**, **28**, and **30**[75]. All data are available from the corresponding author upon request.

References

1. Rodrigues, T., Reker, D., Schneider, P. & Schneider, G. Counting on natural products for drug design. *Nat. Chem.* **8**, 531–541 (2016).
2. Atanasov, A. G. et al. Natural products in drug discovery: advances and opportunities. *Nat. Rev. Drug Discov.* **20**, 200–216 (2021).
3. Frija, L. M. T., Frade, R. F. M. & Afonso, C. A. M. Isolation, chemical, and biotransformation routes of labdane-type diterpenes. *Chem. Rev.* **111**, 4418–4452 (2011).
4. Chen, K. & Baran, P. Total synthesis of eudesmane terpenes by site-selective C–H oxidations. *Nature* **459**, 824–828 (2009).
5. Pronin, S. & Shenvi, R. Synthesis of highly strained terpenes by non-stop tail-to-head polycyclization. *Nat. Chem.* **4**, 915–920 (2012).
6. Mizoguchi, H., Oikawa, H. & Oguri, H. Biogenetically inspired synthesis and skeletal diversification of indole alkaloids. *Nat. Chem.* **6**, 57–64 (2014).
7. Ellerbrock, P., Armanino, N., Ilg, M., Webster, R. & Trauner, D. An eight-step synthesis of epicolactone reveals its biosynthetic origin. *Nat. Chem.* **7**, 879–882 (2015).
8. Kawamura, S., Chu, H., Felding, J. & Baran, P. Nineteen-step total synthesis of (+)-phorbol. *Nature* **532**, 90–93 (2016).
9. Seong, S., Lim, H. & Han, S. Biosynthetically inspired transformation of iboga to monomeric post-iboga alkaloids. *Chem* **5**, 353–363 (2019).
10. Zhang, X. et al. Divergent synthesis of complex diterpenes through a hybrid oxidative approach. *Science* **369**, 799–806 (2020).
11. Godfrey, R., Green, N., Nichol, G. & Lawrence, A. Total synthesis of brevianamide A. *Nat. Chem.* **12**, 615–619 (2020).
12. Huang, Z. & Lumb, J.-P. Mimicking oxidative radical cyclizations of lignan biosynthesis using redox-neutral photocatalysis. *Nat. Chem.* **13**, 24–32 (2021).
13. D'Angelo, K. A., Schissel, C. K., Pentelute, B. L. & Movassaghi, M. Total synthesis of himastatin. *Science* **375**, 894–899 (2022).
14. Pan, L. et al. A general strategy for the synthesis of taxane diterpenes. *Nature* **632**, 543–549 (2024).
15. Dong, H. et al. Chemoenzymatic total synthesis of alchivemycin A. *Nat. Synth.* **3**, 1124–1133 (2024).
16. Alexander, B. W. et al. An oxidative photocyclization approach to the synthesis of *Securiflustra securifrons* alkaloids. *Science* **383**, 849–854 (2024).
17. Li, C. & Shenvi, R. A. Total synthesis of 25 picrotoxanes by virtual library selection. *Nature* **638**, 980–986 (2025).
18. Jørgensen, L. et al. 14-step synthesis of (–)-ingenol from (+)-3-carene. *Science* **341**, 878–882 (2013).
19. Zhou, S., Xia, K., Leng, X. & Li, A. Asymmetric total synthesis of arcutinidine, arcutinine, and arcutine. *J. Am. Chem. Soc.* **141**, 13718–13723 (2019).
20. Kong, L. et al. Total synthesis of (–)-oridonin: an interrupted Nazarov approach. *J. Am. Chem. Soc.* **141**, 20048–20052 (2019).
21. Kamakura, D., Todoroki, H., Urabe, D., Hagiwara, K. & Inoue, M. Total synthesis of talatisamine. *Angew. Chem. Int. Ed.* **59**, 479–486 (2020).
22. Delayre, B., Wang, Q. & Zhu, J. Natural product synthesis enabled by domino processes incorporating a 1,2-rearrangement step. *ACS Cent. Sci.* **7**, 559–569 (2021).
23. Salahi, F., Yao, C., Norton, J. R. & Snyder, S. A. The synthesis of diverse terpene architectures from phenols. *Nat. Synth.* **1**, 313–321 (2022).
24. Gross, B. M., Han, S.-J., Virgil, S. C. & Stoltz, B. M. A convergent total synthesis of (+)-ineleganolide. *J. Am. Chem. Soc.* **145**, 7763–7767 (2023).
25. Xue, Y. et al. Total synthesis of the hexacyclic sesterterpenoid niduterpenoid B via structural reorganization strategy. *J. Am. Chem. Soc.* **146**, 25445–25450 (2024).

26. Heinze, R. C., Lentz, D. & Heretsch, P. Synthesis of strophasterol A guided by a proposed biosynthesis and innate reactivity. *Angew. Chem. Int. Ed.* **55**, 11656–11659 (2016).
27. Zhang, Y. et al. Enantioselective total synthesis of berkeleyone A and preaustinoids. *Angew. Chem. Int. Ed.* **60**, 14869–14874 (2021).
28. Zhang, Z. C. et al. Total synthesis of (+)-cyclobutastellettolide B. *J. Am. Chem. Soc.* **143**, 18287–18293 (2021).
29. Novak, A. J. E., Grigglestone, C. E. & Trauner, D. A biomimetic synthesis elucidates the origin of preuisolactone A. *J. Am. Chem. Soc.* **141**, 15515–15518 (2019).
30. Duecker, F. L., Heinze, R. C. & Heretsch, P. Synthesis of swinhoeisterol A, dankasterone A and B, and periconiastone A by radical framework reconstruction. *J. Am. Chem. Soc.* **142**, 104–108 (2020).
31. Sanchez, A. & Maimone, T. J. Taming shapeshifting anions: total synthesis of ocellatusone C. *J. Am. Chem. Soc.* **144**, 7594–7599 (2022).
32. Zhao, Y. et al. Divergent total syntheses of (−)-crinipellins facilitated by a HAT-initiated Dowd-Beckwith rearrangement. *J. Am. Chem. Soc.* **144**, 2495–2500 (2022).
33. Sun, D. et al. Total synthesis of (−)-retigeranic acid A: a reductive skeletal rearrangement strategy. *J. Am. Chem. Soc.* **145**, 11927–11932 (2023).
34. Wang, W., Feng, S., Wei, Y., Wang, H. & Li, Y. Diastereoselective ring expansion of cyclic ketones enabled by HAT-initiated radical cascade. *Org. Lett.* **25**, 8022–8026 (2023).
35. Steele, R., Fujiu, M. & Sarpong, R. 1,2-Acyl transposition through photochemical skeletal rearrangement of 2,3-dihydrobenzofurans. *Science* **388**, 631–638 (2025).
36. Zhou, J. C. et al. Hapmnioides A–C, rearranged labdane-type diterpenoids from the Chinese liverwort *Haplomitrium mnioides*. *Org. Lett.* **18**, 4274–4276 (2016).
37. Zhou, J. C. et al. Highly rigid labdane-type diterpenoids from a Chinese liverwort and light-driven structure diversification. *Org. Lett.* **17**, 3560–3563 (2015).
38. Zhu, M. et al. Haploides A–G: diterpenoids featuring four new carbon skeletons via non-carbocation-driven skeletal diversification. *Chin. Chem. Lett.* https://doi.org/10.1016/j.cclet.2025.111584 (2025).
39. Asakawa, Y., Toyota, M. & Masuya, T. Phytane- and labdane-type diterpenoids from the liverwort *Haplomitrium mnioides*. *Phytochemistry* **29**, 585–589 (1990).
40. Quinn, R. K. et al. Site-selective aliphatic C–H chlorination using N-chloroamides enables a synthesis of chlorolissoclimide. *J. Am. Chem. Soc.* **138**, 696–702 (2016).
41. Szczepanik, P. M. et al. Convergent assembly of the tricyclic labdane core enables synthesis of diverse forskolin-like molecules. *Angew. Chem. Int. Ed.* **62**, e202213183 (2023).
42. Chen, L., Chen, P., Zhang, X., Zhang, Y. & Jia, Y. Biomimetic synthesis of pallavicinin, neopallavicinin, pallambins A–D, pallaviambins A/B, and pallavicinolides B/C. *Chem* **10**, 2473–2483 (2024).
43. Deng, H. et al. Synthesis of nimbolide and its analogues and their application as poly(ADP-ribose) polymerase-1 trapping inducers. *Nat. Synth.* **3**, 378–385 (2024).
44. Liu, X., Xu, Y., Li, L. & Li, J. Chemoenzymatic oxidation of labdane and formal synthesis of nimbolide. *J. Am. Chem. Soc.* **146**, 26243–26250 (2024).
45. Zhang, Y., Chen, L. & Jia, Y. Total synthesis of pallamolides A–E. *Angew. Chem. Int. Ed.* **63**, e202319127 (2024).
46. Xu, Z.-J. et al. Divergent total synthesis of euphoranginol C, euphoranginone D, *ent*-trachyloban-3β-ol, *ent*-trachyloban-3-one, excoecarin E, and *ent*-16α-hydroxy-atisane-3-one. *Angew. Chem. Int. Ed.* **59**, 19919–19923 (2020).
47. Zong, Y. et al. Enantioselective total syntheses of manginoids A and C and guignardones A and C. *Angew. Chem. Int. Ed.* **60**, 15286–15290 (2021).
48. Gao, Z.-X. et al. Asymmetric synthesis and biological evaluation of platensilin, platensimycin, platencin, and their analogs via a bioinspired skeletal reconstruction approach. *J. Am. Chem. Soc.* **146**, 18967–18978 (2024).
49. Kende, A. S., Fink, D. M., Gougoutas, J. Z. & Malley, M. F. A remarkable synthesis of the bicyclo[4.2.1]nonenedione system. *Synth. Commun.* **46**, 1940–1946 (2016).
50. Xie, Z. F., Suemune, H. & Sakai, K. Synthetic approach to medium-sized cycloalkanones. A one-pot three-carbon ring expansion of carbocyclic β-keto esters. *J. Chem. Soc. Chem. Commun.* **1988**, 612–613 (1988).
51. Grünenfelder, D. C. et al. Enantioselective synthesis of (−)-10-hydroxyacutuminine. *Angew. Chem. Int. Ed.* **61**, e202117480 (2022).
52. Jauch, J. A short total synthesis of kuehneromycin A. *Angew. Chem. Int. Ed.* **39**, 2764–2765 (2000).
53. Uwamori, M., Osada, R., Sugiyama, R., Nagatani, K. & Nakada, M. Enantioselective total synthesis of cotylenin A. *J. Am. Chem. Soc.* **142**, 5556–5561 (2020).
54. Chen, X. et al. Enantiocontrolled total synthesis of (−)-retigeranic acid A. *J. Am. Chem. Soc.* **145**, 13549–13555 (2023).
55. Ma, Z. et al. Asymmetric syntheses of sceptrin and massadine and evidence for biosynthetic enantiodivergence. *Science* **346**, 219–224 (2014).
56. Nicolaou, K. C., Snyder, S. A., Montagnon, T. & Vassilikogiannakis, G. The Diels–Alder reaction in total synthesis. *Angew. Chem. Int. Ed.* **41**, 1668–1698 (2002).
57. Fadel, M. & Carreira, E. M. Enantioselective total synthesis of (+)-pedrolide. *J. Am. Chem. Soc.* **145**, 8332–8337 (2023).
58. Ji, J. et al. Total synthesis of vilmoraconitine. *J. Am. Chem. Soc.* **145**, 3903–3908 (2023).
59. Zhang, W., Yu, P. C., Feng, C. Y. & Li, C. C. Asymmetric total synthesis of pedrolide. *J. Am. Chem. Soc.* **146**, 2928–2932 (2024).
60. Li, Y., Xue, Q., Zhao, X. & Ma, D. Total syntheses of diepoxy-*ent*-kaurane diterpenoids enabled by a bridgehead-enone-initiated intramolecular cycloaddition. *J. Am. Chem. Soc.* **147**, 1197–1206 (2025).
61. Stratakis, M. & Orfanopoulos, M. Regioselectivity in the ene reaction of singlet oxygen with alkenes. *Tetrahedron* **56**, 1595–1615 (2000).
62. Wu, Y. et al. Facile cleavage of triethylsilyl (TES) ethers using o-Iodoxybenzoic acid (IBX) without affecting *tert*-butyldimethylsilyl (TBS) ethers. *Org. Lett.* **4**, 2141–2144 (2002).
63. Otera, J., Danoh, N. & Nozaki, H. Novel template effects of distannoxane catalysts in highly efficient transesterification and esterification. *J. Org. Chem.* **56**, 5307–5311 (1991).
64. Shimakawa, T., Nakamura, S., Asai, H., Hagiwara, K. & Inoue, M. Total synthesis of puberuline C. *J. Am. Chem. Soc.* **145**, 600–609 (2023).
65. Reusch, W. et al. Preparation of fused-ring cyclopropanol derivatives by reductive cyclization of bicyclic enediones related to the Wieland-Miescher ketone. *J. Am. Chem. Soc.* **99**, 1953–1958 (1977).
66. Hong, B. et al. Photoinduced skeletal rearrangements reveal radical-mediated synthesis of terpenoids. *Chem* **5**, 1671–1681 (2019).
67. Kärkäs, M. D., Porco, J. A. & Stephenson, C. R. J. Photochemical approaches to complex chemotypes: applications in natural product synthesis. *Chem. Rev.* **116**, 9683–9747 (2016).
68. Poirel, C., Renard, P.-Y. & Lallemand, J.-Y. Stereoselective access to polyfunctionalized decalins. *Tetrahedron Lett.* **35**, 6485–6488 (1994).

69. Cheng, S., Dong, C., Ma, Y., Xu, X. & Zhao, Y. Skeletal transformations of terpenoid forskolin employing an oxidative rearrangement strategy. *J. Org. Chem.* **89**, 5741–5745 (2024).
70. Betinol, I. O., Kuang, Y., Mulley, B. P. & Reid, J. P. Controlling stereoselectivity with noncovalent interactions in chiral phosphoric acid organocatalysis. *Chem. Rev.* **125**, 4184–4286 (2025).
71. Crimmins, M. T. et al. Total synthesis of (±)-ginkgolide B. *J. Am. Chem. Soc.* **121**, 10249–10250 (1999).
72. Zhang, W. et al. Total synthesis of hybridaphniphylline B. *J. Am. Chem. Soc.* **140**, 4227–4231 (2018).
73. Davis, R. L., Leverett, C. A., Romo, D. & Tantillo, D. J. Switching between concerted and stepwise mechanisms for dyotropic rearrangements of β-lactones leading to spirocyclic, bridged γ-butyrolactones. *J. Org. Chem.* **76**, 7167–7174 (2011).
74. Leverett, C. A. et al. Dyotropic rearrangements of fused tricyclic β-lactones: application to the synthesis of (−)-curcumanolide A and (−)-curcumalactone. *J. Am. Chem. Soc.* **134**, 13348–13356 (2012).
75. Song, J.-G. et al. Crystalline mate for structure elucidation of organic molecules. *Chem* **10**, 924–937 (2024).

Acknowledgements

We thank M.-Z. Zhu and J.-Z. Zhang of the department of natural products chemistry at Shandong university for assistance in the NMR analysis. This work was financially supported by the National Natural Science Foundation of China (grant no. 82293682 and 82173703 to H.-X.L., grant no. 82273807 to Z.-J.X.), and Shandong Provincial Natural Science Foundation (grant no. ZR2022YQ74 to Z.-J.X.).

Author contributions

H.-X.L. and Z.-J.X. conceived the project, guided the studies, and wrote the manuscript. Z.-X.G. completed the synthesis of these seven *Haplomitrium* diterpenoids. C.S., H.-X.Z., Y.-Q.Z., X.-X.C., and X.-Y.L. participated in material preparation. A.-X.C. provided further X-ray crystallographic analysis. All of the authors contributed to the analysis of the results.

Competing interests

The authors declare no competing interests.

Additional information

Supplementary information The online version contains supplementary material available at https://doi.org/10.1038/s41467-025-66093-0.

Correspondence and requests for materials should be addressed to Ze-Jun Xu or Hong-Xiang Lou.

Peer review information *Nature Communications* thanks Hanfeng Ding and the other anonymous reviewer(s) for their contribution to the peer review of this work. A peer review file is available.